

Dose compensation based on biological effectiveness due to interruption time for photon radiation therapy

Abstract

5 **Objectives:** To evaluate the biological effectiveness of dose associated with interruption time; and propose the dose compensation method based on biological effectiveness when an interruption occurs during photon radiation therapy.

Methods: The lineal energy distribution for human salivary gland tumor was calculated by Monte Carlo simulation using a photon beam. The biological dose (D_{bio}) was estimated
10 using the microdosimetric kinetic model. The dose compensating factor with the physical dose for the difference of the D_{bio} with and without interruption (Δ) was derived. The interruption time (τ) was varied to 0.1, 0.2, 0.3, 0.4, 0.5, 1, 2, 3, 4, 5, 10, 20, 30, 40, 50, 75, and 120 min. The dose per fraction and dose rate varied from 2 to 8 Gy and 0.1 to 24 Gy/min, respectively.

15 **Results:** The maximum Δ with 1 Gy/min occurred when the interruption occurred at half the dose. The Δ with 1 Gy/min at half of the dose was over 3% for $\tau \geq 20$ min for 2 Gy, $\tau = 10$ min for 5 Gy, and $\tau = 10$ min for 8 Gy. The maximum difference of the Δ due to the dose rate was within 3% for 2 and 5 Gy, and achieving values of 4.0% for 8

Gy. The dose compensating factor was larger with a high dose per fraction and high-dose

20 rate beams.

Conclusion: A loss of biological effectiveness occurs due to interruption. Our proposal method could correct for the unexpected decrease of the biological effectiveness caused by interruption time.

25 **Advances in knowledge:** For photon radiotherapy, the interruption causes the sublethal damage repair (SLDR). The current study proposed the dose compensation method for the decrease of the biological effect by the interruption.

Keywords: Microdosimetric kinetic model, interruption time, dose compensation model

30

1. Introduction

Recent technological advancements in radiation therapy, such as immobilization, the use of a linear accelerator, imaging, a treatment planning system, and the ability to compensate for respiratory motion could utilize intensity-modulated radiation therapy (IMRT). IMRT delivers precise radiation doses to a tumor while minimizing the dose to the surrounding normal tissue. However, these techniques are complex and could require more time to deliver the dose than conventional radiation therapy. IMRT uses several beams and segments (apertures) that are shaped using a multileaf collimator. The dose is delivered either statically or dynamically through the step-and-shoot mode. For multi-beam radiation therapy, the delivery time will frequently increase proportionally to the complexity of the treatment technique. For lung or liver cancer patients, respiratory control such as respiratory gating or breath-holding techniques is needed to suppress the organ or tumor motion [1-2]. Additionally, linac failure causes unscheduled downtime. In some cases, it was necessary to transfer patients to other linacs [3]. Consequently, the doses were delivered intermittently. IMRT could require up to 15 min and SBRT requires 30 min or longer [4]. Unscheduled downtime increases the interruption time. These interruption periods in treatment significantly increase the possibility of error and intrafraction motion. It could be questioned from the therapeutic point of view whether

50 the radiation dose delivered with interruption is equivalent to that administered without interruption.

The effect of the interruption time was studied by Elkind et al. who demonstrated that cell killing tends to decrease with increased delivery time. This effect was primarily related to sublethal damage repair (SLDR) [5]. Mu et al. investigated the effect of
55 interruption time through in vitro experiments. The effect of prolonging the fraction time that includes the beam-on time and interruption times in treatment is underestimated by biological models [6].

For the estimation of cell survival and the calculation of the biological equivalent dose, the linear-quadratic (LQ) model has been widely used [7, 8]. However, the LQ
60 model does not represent the effect of the SLDR by the prolonged delivery time and dose rate effect explicitly. The microdosimetric-kinetic (MK) model is possible to evaluate the surviving fraction in terms of microdosimetry [9, 10]. The MK model expresses the difference in radiation energy by taking into account the spatial distribution of the energy deposition of radiation [11]. Moreover, the MK model is possible to be incorporated the
65 biological effect of the SLDR. Matsuya et al evaluated the survival curve with the experimental data and the fitted data by the LQ and MK models. The MK model which incorporated the dose rate expressed the SF accurately [12]. Inaniwa et al. evaluated the

effect of longer periods of dose delivery for carbon-ion radiotherapy using the MK model [13]. They demonstrated that the biological effect of a planned dose can decrease by 20%

70 or more than the curative dose if the interruption time extends to 30 min or longer.

Although our previous study evaluated the effect of delivery time under a continuous photon beam, the effect of the interruption time was not assessed [14]. For photon therapy, the decrease in the biological effect associated with the interruption time, i.e., a decrease in cell killing could also occur.

75 The current study aims to reveal the effect of biological dose difference with and without interruption by a photon beam. Additionally, two types of dose compensation methods to achieve biologically equivalent dose per fraction with interruption are proposed.

2. Materials and methods

2.1. Survival fraction in the MKM

Hawkins et al proposed the MKM, the surviving fraction of cells can be predicted from the dose by a “domain” that the cell nucleus was divided [10]. The specific energy which is the dose absorbed by any individual domain is defined as z . The average of z for the entire population is defined as D which is the macroscopically measured dose. It is assumed that the primary lesions in the domain have two types. Type I is a potentially lethal lesion, which is assumed to correspond to a clustered DNA damage that induces chromosome aberrations and it is difficult to repair. A type II lesion occurred after the irradiation of the domains. According to their transformations, the type II lesions are classified into four categories: (1) be converted to a lethal unrepairable lesion at a constant rate a through first-order process; (2) form a lethal unrepairable lesion through second-order process b_d by combining with another type II lesion in the same domain; (3) be repaired at constant rate c through first-order process; and (4) persist for a length of time t_r , after which it becomes lethal and unrepairable. Type I and type II lesions are created with a proportional to the z with the k_{dI} and λ_d , respectively. These are expressed as following equations:

$$\frac{dx_{II}}{dt} = k_{dI}z - (a + c)x_{II} - 2b_dx_{II}^2, \quad (1)$$

$$\frac{dx_I}{dt} = \lambda_d \dot{z} + ax_{II} + b_d x_{II}^2, \quad (2)$$

where x_I and x_{II} are the mean number of type I and type lesions per domain at z . the

Brenner et al assumed that the potentially lethal lesion repair rate, which was defined as

100 $(a + c)$, was equivalent to the primary rate λ which was obtained by the DNA repair

half-time $T_{1/2}$ [15].

$$a + c = \frac{\ln 2}{T_{1/2}}, \quad (3)$$

When a population of cells exposed to D at time $t = 0$ and a domain absorbs z from this

irradiation, Eq. (1) becomes

105
$$x_{II} = k_d \dot{z} - (a + c)x_{II}, \quad (4)$$

Inaniwa et al showed that the \dot{z} that is the time derivative of z is given stochastically

[16]. The average of x_I at $t \rightarrow \infty$ taken over all domains of the irradiated cell population

including all values of z , x_I , is estimated stochastically, and the probability of having no

lethal lesion in the domain s_d over the population that the survival fraction is then

110 determined by

$$\ln s_d = -x_I, \quad (5)$$

Consider a population of cells exposed to macroscopic dose D at time $t = 0$ and a domain

within the population absorbs z . Kase et al derived the survival fraction of cells after the

irradiation [17].

$$-lnS = (\alpha_0 + z_{1,D}\beta_0)D + \beta_0 D^2, \quad (6)$$

The $z_{1,D}$ denotes the dose mean specific energy by single energy deposition events. The α_0 is the proportional factor to D [Gy^{-1}] and β_0 is the proportionality factor to D^2 [Gy^{-2}], which are obtained by the survival fraction in the LQ model. Additionally, Kase et al converted the $z_{1,D}$ to the following equation to measure [17].

$$z_{1,D} = \frac{y_D}{\rho\pi r_d^2}, \quad (7)$$

where y_D , dose mean energy (keV/ μm), is given by

$$y = \frac{\varepsilon}{l}, \quad (8)$$

$$y_D = \frac{\int y^2 f(y) dy}{\rho\pi r_d}, \quad (9)$$

where y is the lineal energy, l is the mean chord length expressed as two-thirds times the

domain diameter, ε is the energy deposited in a domain. The values of r_d and ρ , which are

the radius and of the domain and the density of the domain are 0.23 μm and 1.0 g/cm^3 ,

respectively. The domain size was assumed to be composed of spherical sites with

diameters from 1 nm to 1 μm . An analytical function was developed based on this result.

Okamoto et al obtained the domain size from the slope of the linear function, which was

used in the current study [18]. The $f(y)$ is the probability density of lineal energy. The

lineal energy is a stochastic quantity. When particles interact, they can release different

quantities of energy which generate a broad spectrum of the lineal energy with different

probabilities. The value of the distribution function, $F(y)$, is the probability that the lineal energy is equal to or less than y . The probability density $f(y)$ is the derivative of $F(y)$ with respect to y .

$$f(y) = \frac{dF(y)}{dy} \quad (10)$$

The linear energy distribution, $f(y)$, is independent of the absorbed dose or dose rate. The dose distribution, $d(y)$, can be determined from the above distribution and is the normalized distribution of the product $yf(y)$ which represents the relative contribution of events with magnitude y to the dose. Let $D(y)$ be the fraction of absorbed dose delivered with lineal energy less than or equal to y , then the dose probability density, $d(y)$, is the derivative of $D(y)$ with respect to y

$$d(y) = \frac{dD(y)}{dy} \quad (11)$$

2.2. Lineal energy distribution in PHITS

TrueBeam linear accelerators (Varian Medical Systems, Palo Alto, USA) with a 6-MV x-ray beam was modeled in the Particle and Heavy Ion Transport Code System (PHITS). Phase space files located above the secondary jaw for Monte Carlo users were provided by Varian [19]. The below phase-space files were created using BEAMnrc,

which is built on the EGSnrc platform [20]. These phase space files created by BEAMnrc were transferred to the PHITS system, which performed dose calculation. The virtual homogeneous phantom ($20 \times 20 \times 20 \text{ cm}^3$) was created; the beam was used for a $5 \times 5 \text{ cm}^2$ field size at SSD = 90 cm using PHITS. For the physical dose calculation, the calculation grid size used was 2 mm. The photon and electron cut-off energies were set to 0.01 MeV and 0.7 MeV, respectively. The number of photon histories was 2.0×10^8 in BEAMnrc and 4.0×10^9 in PHITS, respectively. The validation of the Monte Carlo calculations was performed in our previous study, where we compared simulation and measurement results [21]. The Monte Carlo calculation and the corresponding measurement in the chamber matched within 1.0%. Using the T-SED function of PHITS, the y distribution with a 6-MV x-ray beam was calculated [22].

2.3. Biological dose with MKM for interruption

For continuous irradiation without interruption, Inaniwa et al derived the survival fraction of cells after the irradiation [13].

$$-\ln S = (\alpha_0 + z_{1,D}\beta_0)D + \beta'D^2 \quad (12)$$

$$\beta' = \frac{2\beta}{(a+c)^2T^2} \left[(a+c)T \frac{(1+e^{-2(a+c)t_r})}{(1-e^{-2(a+c)t_r})} - 1 + \frac{e^{-(a+c)T}(1-e^{-2(a+c)(t_r-T)})}{(1-e^{-2(a+c)t_r})} \right] \quad (13)$$

where the T is the delivery time during irradiation, which is calculated with the dose rate

170 DR as follows:

$$T = \frac{D}{DR} \quad (14)$$

The current study simulated the lineal energy distribution and calculate the y_d with

PHITS. Thus, the Eq. (6) is converted with Eq. (7) as follows:

$$-\ln S = \left(\alpha_0 + \frac{y_d}{\rho \pi r_d} \beta_0 \right) D + \beta' D^2 \quad (15)$$

175 The survival fraction with interruption is calculated stochastically following steps similar

to those described by Inaniwa et al. [16]. It was calculated as:

$$\ln S = -(\alpha_0 + z_{1,D} \beta_0) D_1 - (\alpha_0 + z_{2,D} \beta_0) D_2 - \beta_1 D_1^2 - \beta_2 D_2^2 - \beta_3 D_1 D_2 \quad (16)$$

where S is the survival fraction that is dependent on the dose. The number of the

interruptions is one. Conventionally radiotherapy has performed with a total dose of 60–

180 70 Gy in 2Gy/fr [23]. The hypofraction radiotherapy scheme is also used in clinical [24,

25]. On the other hand, a recent study showed that in addition to the direct cell death,

indirect cell death through vascular damage occurs when tumors are exposed to high dose

hypo-fractionated irradiation [26]. From these clinical protocols, the current study used

the dose per fraction (D) of 2-8 Gy. The D is calculated as:

$$185 \quad D = D_1 + D_2 \quad (17)$$

The D_1 and D_2 are the physical dose at first and second irradiations. The D_1 and D_2 in the D are separated using the interrupted dose fraction (IDF), which is defined as:

$$IDF = \frac{D_1}{D} \times 100 \quad (18)$$

The IDF was changed from the 10%, 30%, 50%, 70%, and 90%.

The $z_{1,D}$ and $z_{2,D}$ are dose mean specific energies absorbed by a domain in a single event during the first and second irradiations, respectively. The current study used the photon beam which energy loss due to the depth is small. Moreover, the current study simulated the virtual phantom and a single field is used. Thus, the $z_{1,D}$, and $z_{2,D}$ are used the same value. Moreover, the survival fraction can be converted with Eq. (9) as follows:

$$\ln S = -\left(\alpha_0 + \frac{\gamma_D}{\rho \pi r_d} \beta_0\right) D_1 - \left(\alpha_0 + \frac{\gamma_D}{\rho \pi r_d} \beta_0\right) D_2 - \beta_1 D_1^2 - \beta_2 D_2^2 - \beta_3 D_1 D_2 \quad (19)$$

The coefficients β_1 , β_2 , and β_3 are provided by:

$$\beta_1 = \frac{2\beta}{(a+c)^2 T_1^2} \left[(a+c) T_1 \frac{(1+e^{-2(a+c)t_r})}{(1-e^{-2(a+c)t_r})} - 1 + \frac{e^{-(a+c)T_1} (1-e^{-2(a+c)(t_r-T_1)})}{(1-e^{-2(a+c)t_r})} \right] \quad (20)$$

$$\beta_2 = \frac{2\beta}{(a+c)^2 T_2^2} \left[(a+c) T_2 \frac{(1+e^{-2(a+c)t_r})}{(1-e^{-2(a+c)t_r})} - 1 + \frac{e^{-(a+c)T_2} (1-e^{-2(a+c)(t_r-T_2)})}{(1-e^{-2(a+c)t_r})} \right] \quad (21)$$

$$\beta_3 = \frac{2\beta}{(a+c)^2 T_1 T_2 (1-e^{-2(a+c)t_r})} \left\{ e^{-(a+c)(\tau+T_2)} + e^{-(a+c)\tau} - e^{-(a+c)(T_1+\tau+T_2)} + e^{-(a+c)(2t_r-\tau-T_2)} - e^{-(a+c)(2t_r-T_1-\tau-T_2)} - e^{-(a+c)(2t_r-\tau)} + e^{-(a+c)(2t_r-\tau-T_1)} \right\}, \quad (22)$$

where, the T_1 and T_2 are delivery time at first and second irradiations, which are

205 calculated with the dose rate DR as follows:

$$T_1 = \frac{D_1}{DR} \quad (23)$$

$$T_2 = \frac{D_2}{DR} \quad (24)$$

In total body irradiation, the dose rate is a factor that influences biological effects, and it is accepted practice to keep the dose rate between 0.05 and 0.10 Gy/min [27]. For a flattening filter-free beam, the dose rates of up to 24 Gy/min could be used [28]. From above, the DR ranged from 0.1 to 24 Gy/min. These equations were defined under the condition of $\tau < t_r$. Here, the t_r with HSG tumor is used 2.28h, which is referenced from a previous study [16]. The τ was defined as the interruption time. The range of the τ was assumed the clinical treatment. Kuterdem et al reported the delivery time and beam-on time of the dynamic multi-leaf collimation in IMRT and it was an average beam pause duration in dynamic of 7 seconds [29]. For Volumetric Modulated Arc Therapy (VMAT) treatments, mechanical motion time was assumed to be 30 seconds, accounting for the collimator rotation between gantry arcs [30]. Moreover, an interruption could occur from unscheduled downtime with machine failures. Although the interruption might occur over 120 min, the lesion becomes the lethal and unrepairable after the t_r . Thus, the current study assumed that the maximum interruption time is used 120 min which is below the t_r . From above, the interruption time (τ) was varied to 0.1, 0.2, 0.3, 0.4, 0.5, 1, 2, 3, 4, 5,

10, 20, 30, 40, 50, 75, and 120 min.

The biological dose (D_{bio}) proposed by Inaniwa et al [11] was computed as:

$$D_{bio} = \left[-\frac{\alpha_0}{2\beta} + \sqrt{\left(\frac{\alpha_0}{2\beta}\right)^2 - \frac{\ln S}{\beta}} \right] \quad (25)$$

Using Eq. 15, D_{bio} with and without interruption can be converted as follows:

$$D_{bio}^{w/o} = \left[-\frac{\alpha_0}{2\beta_0} + \sqrt{\left(\frac{\alpha_0}{2\beta_0}\right)^2 + \frac{\left(\alpha_0 + \frac{y_D}{\rho\pi r_d}\beta'\right)D + \beta'D^2}{\beta_0}} \right] \quad (26)$$

$$D_{bio}^{with} = \left[-\frac{\alpha_0}{2\beta_0} + \sqrt{\left(\frac{\alpha_0}{2\beta_0}\right)^2 + \frac{\left(\alpha_0 + \frac{y_D}{\rho\pi r_d}\beta'\right)D_1 + \left(\alpha_0 + \frac{y_D}{\rho\pi r_d}\beta'\right)D_2 + \beta_1 D_1^2 + \beta_2 D_2^2 + \beta_3 D_1 D_2}{\beta_0}} \right] \quad (27)$$

where $D_{bio}^{w/o}$ and D_{bio}^{with} are the biological doses without and with interruption,

respectively. Table 1 shows the cell parameters of the human salivary gland (HSG) tumor cells which referenced from a previous study and the calculated y_D values for the 6-MV

x-ray beam, which was the dose-mean lineal energy [18]. The HSG tumor cell is a standard reference cell line to compare RBE mutually for proton facilities in Korea, Japan, etc. [31]. At cell culture, eagle's minimum essential medium (M4655, Sigma) supplemented with 10% fetal bovine serum and antibiotics (100 U/ml penicillin and 100 μ g/ml streptomycin) was used. Harvested cells were seeded in T25 flasks at about $2.0 \times$

240 10^5 cells/flask with 5 ml of the medium, and incubated in a 5% CO₂ incubator at 37°C
for 2 days prior to irradiation with 6-MV x-ray photon beam. The depths from the
phantom surface to cells was 100 mm water equivalent depth. Okamoto et al counted
colonies consisting of more than 50 cells as the number of viable cells. The calculated y_D
value was agreed with the measurement value in a previous study [18].

245

Table 1. Calculation parameters [parameters (mean and standard deviation (SD))]. The α_0
is the proportional factor to D [Gy^{-1}], β_0 is the proportionality factor to D^2 [Gy^{-2}], y_D is
the dose-mean lineal energy, and $T_{1/2}$ is the DNA repair half-time.

Parameters	Mean	SD
α_0 (Gy^{-1})	0.175	0.023
β_0 (Gy^{-2})	0.033	-
$T_{1/2}$ (min)	22	-
y_D (keV/ μm)	2.32	0.04

250

2.4. Biological dose difference for interruption

From a previous study, the D_{bio} for interruption was underestimated when compared with the D_{bio} without interruption [16]. Our study assumed that the

underestimated D_{bio} should be supplied in addition to the prescribed dose when the

interruption occurred. Thus, the biological dose difference (Δ) was estimated according to the following definition: the deviation of the D_{bio} without interruption, and that with interruption, divided by the D_{bio} with interruption.

$$\Delta = \frac{D_{bio}^{w/o} - D_{bio}^{with}}{D_{bio}^{with}} \quad (28)$$

2.5. Dose compensating factor for the biological dose with interruption

The biological dose with an interruption can be corrected with the Δ and the biological dose without interruption, as follows;

$$D_{bio}^{w/o} = (1 + \Delta) \times (D_{1,bio}^{with} + D_{2,bio}^{with}) \quad (29)$$

where, the $D_{1,bio}^{with interruption}$ and $D_{2,bio}^{with interruption}$ are the biological dose with interruption at first and second irradiation, respectively. In the photon therapy treatment, the prescription has been performed with the physical dose. Thus, the Δ should be corrected with the physical dose and the compensating factor (f). The current study

suggests the two types of dose compensating methods based on the biological dose difference with and without interruption, as shown in Fig. 1. One is that the second-irradiation method in which the compensating is performed for D_2 after the first irradiation. The other is the additional dose method which the additional dose with the corrected the D_1 immediately after the first and second irradiation is provided.

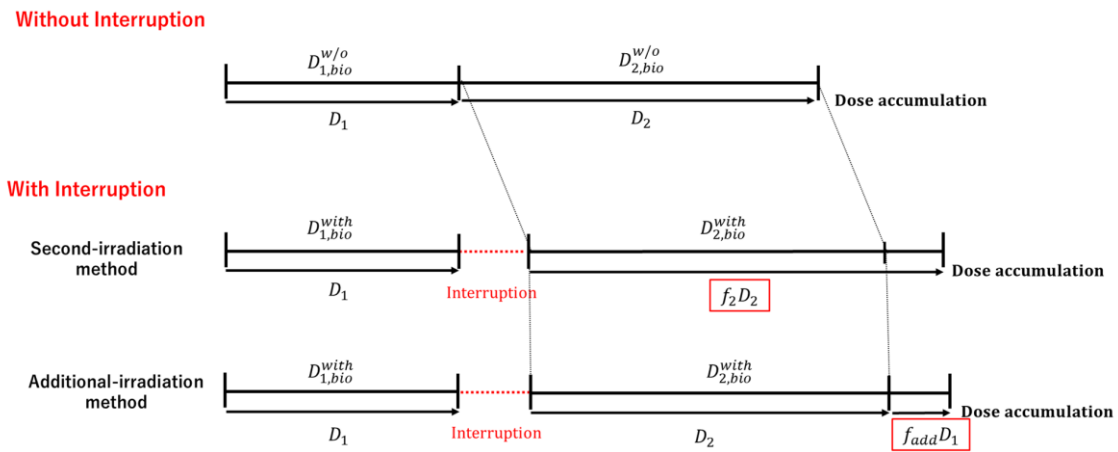


Fig. 1 Two types of dose compensating methods: One is second-irradiation method that the decrease of the biological effectiveness with interruption is corrected with the D_2 in the second irradiation. The other is the additional-irradiation method that the decrease of the biological effectiveness with interruption is compensated with the additional dose.

2.5.1 Dose compensating factor in the second-irradiation method

It was assumed that the biological dose without interruption was equivalent to

be the sum of the biological dose at first-irradiation with interruption and the biological compensated dose ($cD_{2,bio}^{with}$) for second-irradiation with interruption.

$$D_{bio}^{w/o} = D_{1,bio}^{with} + cD_{2,bio}^{with} \quad (30)$$

From the Eq. (29) and (30), the $cD_{2,bio}^{with}$ is derived as:

$$cD_{2,bio}^{with} = \Delta \times D_{1,bio}^{with} + D_{2,bio}^{with} \times (\Delta + 1) \quad (31)$$

The $cD_{2,bio}^{with}$ can be converted to the physical dose ($D_{2,phy}^{w/o}$) with Eq. (26), which is given by:

$$D_{2,phy}^{w/o} = \frac{-\left(\frac{\alpha_0}{\beta} + \frac{\beta_0}{\beta} \frac{y_D}{\rho \pi r_d}\right) + \sqrt{\left(\frac{\alpha_0}{\beta} + \frac{\beta_0}{\beta} \frac{y_D}{\rho \pi r_d}\right)^2 + 4 \frac{\beta_0}{\beta} cD_{2,bio}^{with} \left(cD_{2,bio}^{with} + \frac{\alpha_0}{\beta_0}\right)}}{2} \quad (32)$$

The dose compensating factor based on biological effectiveness at second irradiation with interruption (f_2) is derived as:

$$f_2 = \frac{D_{2,phy}^{w/o}}{D_2} \quad (33)$$

2.5.2 Dose compensating factor for the additional dose method

It was assumed that the additional dose with the corrected the D_1 ($cD_{1,bio}^{with}$) was provided immediately after the first and second irradiation to be equivalent to the biological dose without interruption. It can be expressed with Eq. (29).

$$D_{bio}^{w/o} = D_{1,bio}^{with} + D_{2,bio}^{with} + cD_{1,bio}^{with} \quad (34)$$

The $cD_{1,bio}^{with}$ can be converted to the physical dose ($D_{1,phy}^{w/o}$) with Eq. (26), which is given by:

305

$$D_{1,phy}^{w/o} = \frac{-\left(\frac{\alpha_0}{\beta} + \frac{\beta_0}{\beta} \frac{y_D}{\rho \pi r_d}\right) + \sqrt{\left(\frac{\alpha_0}{\beta} + \frac{\beta_0}{\beta} \frac{y_D}{\rho \pi r_d}\right)^2 + 4 \frac{\beta_0}{\beta} cD_{1,bio}^{with} \left(cD_{1,bio}^{with} + \frac{\alpha_0}{\beta_0}\right)}}{2} \quad (35)$$

The dose compensating factor based on biological effectiveness at additional-irradiation with interruption (f_{add}) is derived as:

$$f_{add} = \frac{D_{1,phy}^{w/o}}{D_1} \quad (37)$$

310

3. Results

3.1. Survival fraction with a different fraction of the interrupted dose

Figure 2 shows the survival fraction as a function of interruption time at the IDF of 10% and 50% with 1 Gy/min for the D of 2–8 Gy. The survival fraction increases with an increase in the interruption time. The survival fraction at the IDF of 50% is larger than that 10%. The difference of the survival fraction at the IDF of 10% and 50% for 8 Gy is larger.

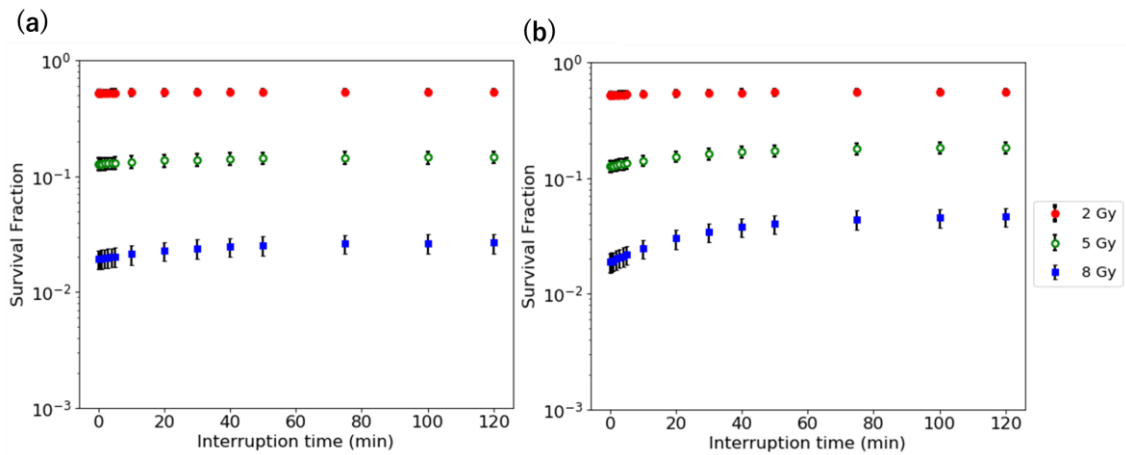


Fig. 2 Survival fraction vs. interruption time at the IDF of (a) 10% and (b) 50% for the D of 2–8 Gy.

3.2. Biological dose difference with different fraction of the interrupted dose

Figure 3 shows the Δ as a function of interruption time with 1 Gy/min for the D of 2–8 Gy. For the IDF of 10%–90%, the maximum Δ occurs when the interruption is at an IDF of 50%. The Δ at the IDF of 10% and 30% are identical to that at the IDF of 90% and 70%, respectively. The smallest Δ value occurs when the interruption is at the IDF of 10% and 90%. The maximum Δ is larger with a higher dose. Its largest value is 17.4% at the IDF of 50% for 8 Gy. The minimum interruption time of the $\Delta \times 100$ that was over 3% occurs with $\tau = 20$ min for 2 Gy, $\tau = 10$ min for 5 Gy, and $\tau = 10$ min for 8 Gy, respectively. For 2 Gy, the $\Delta \times 100$ is within 10% with an interruption time of 0–120 min. Moreover, the maximum Δ for 5–8 Gy is larger with a higher dose, which is over 10%.

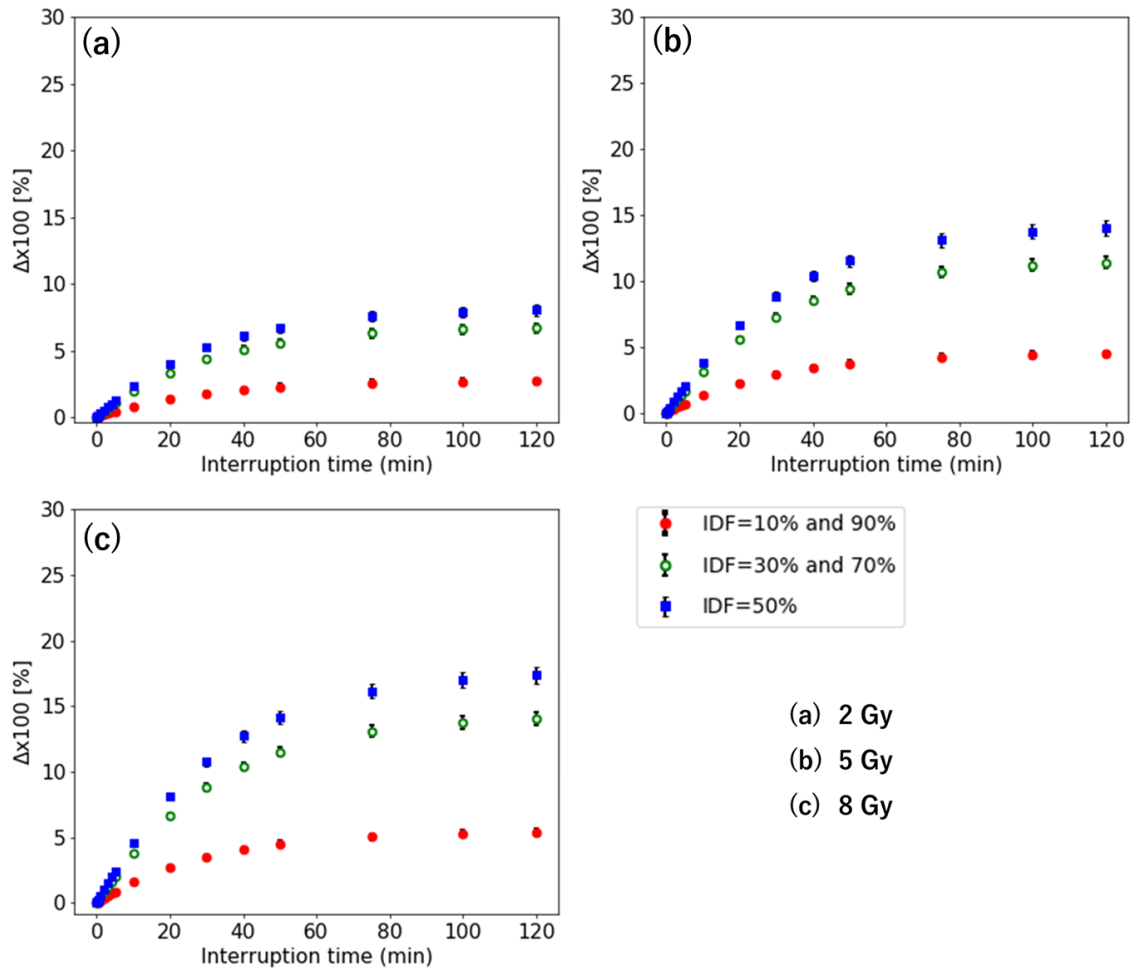


Fig. 3 Δ when the interruption occurs at the IDF of 10%–90% for the D of (a) 2 Gy, (b) 5 Gy, and (c) 8 Gy.

340

3.3. Biological dose difference with a different dose rate for interruption

Figure 4 shows the Δ vs. interruption time at the IDF of 50% with 0.5–24 Gy/min for the D of 2–8 Gy. The Δ with low-dose rate is smaller. There is a small difference in the $\Delta \times 100$ with 0.5–24 Gy/min within 3% for 2 and 5 Gy. The maximum

345 difference of the $\Delta \times 100$ is 4.0% for 8 Gy with $\tau = 120$ for 20 Gy.

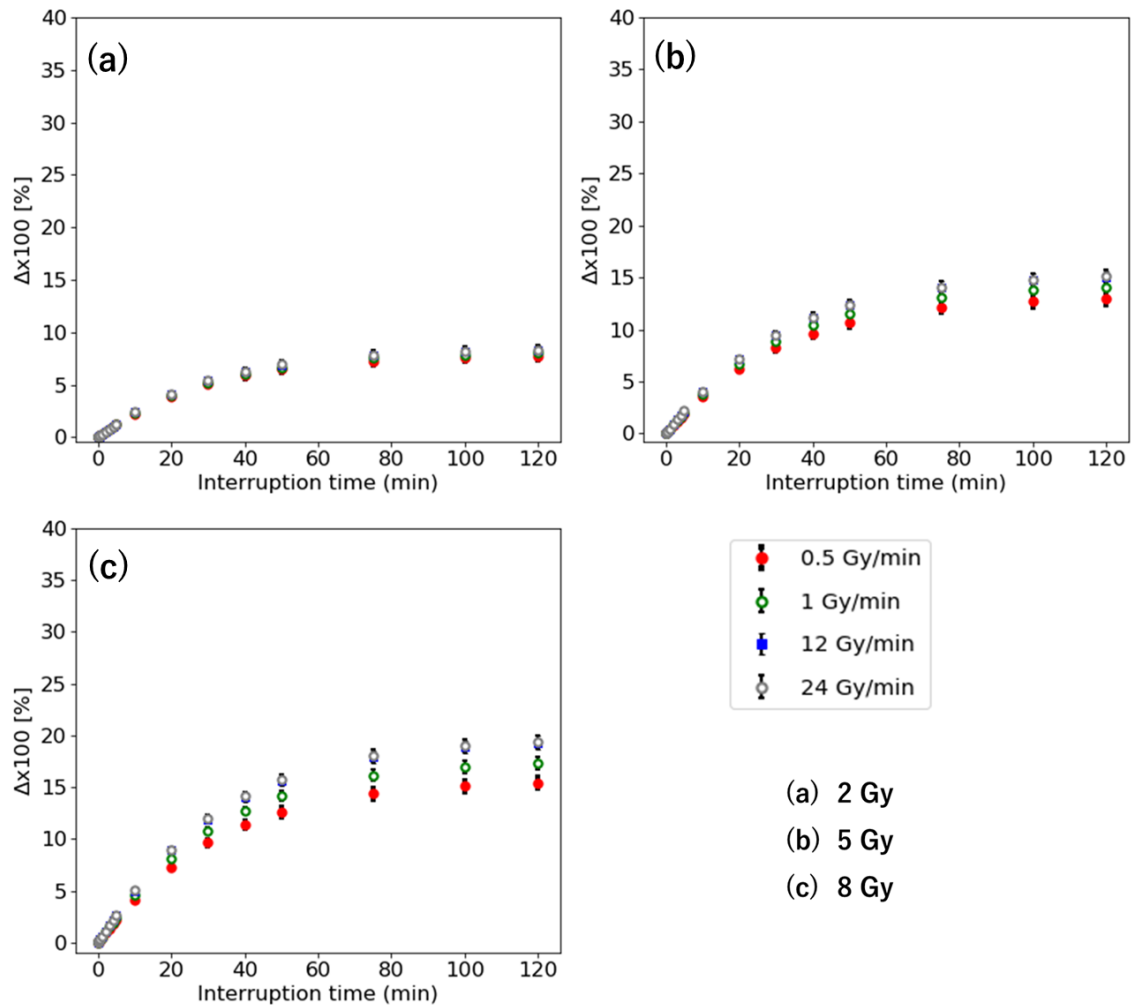


Fig. 4 Δ vs. interruption time with 0.5–24 Gy/min for the D of (a) 2 Gy, (b) 5 Gy, and

350 (c) 8 Gy.

3.4. Dose compensating factor with different fraction of the interrupted dose

Figures 5 and 6 show the f_2 and f_{add} in the second-irradiation method and additional-

irradiation method with 1 Gy/min for the D of 2–8 Gy. The f_2 and f_{add} are larger

355 with a high-dose rate, which indicates a similar result with the Δ . The higher dose has

higher f_2 and f_{add} . Its largest values are 1.50 for the f_2 at an IDF of 90% and 0.49

for the f_{add} at an IDF of 10% for 8 Gy. The maximum f_2 and f_{add} are larger with a

higher dose per fraction.

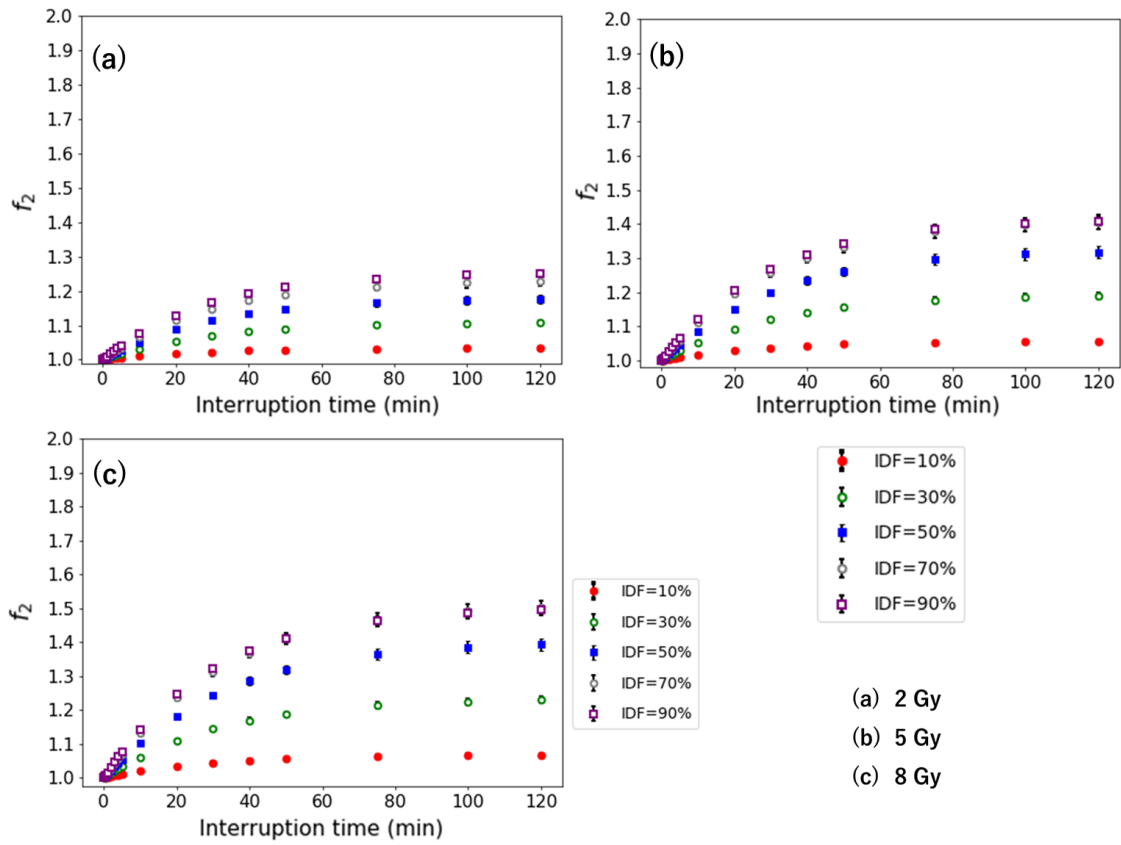


Fig. 5 f_2 when the interruption occurs at the IDF of 10%–90% for the D of (a) 2 Gy,

(b) 5 Gy, and (c) 8 Gy.

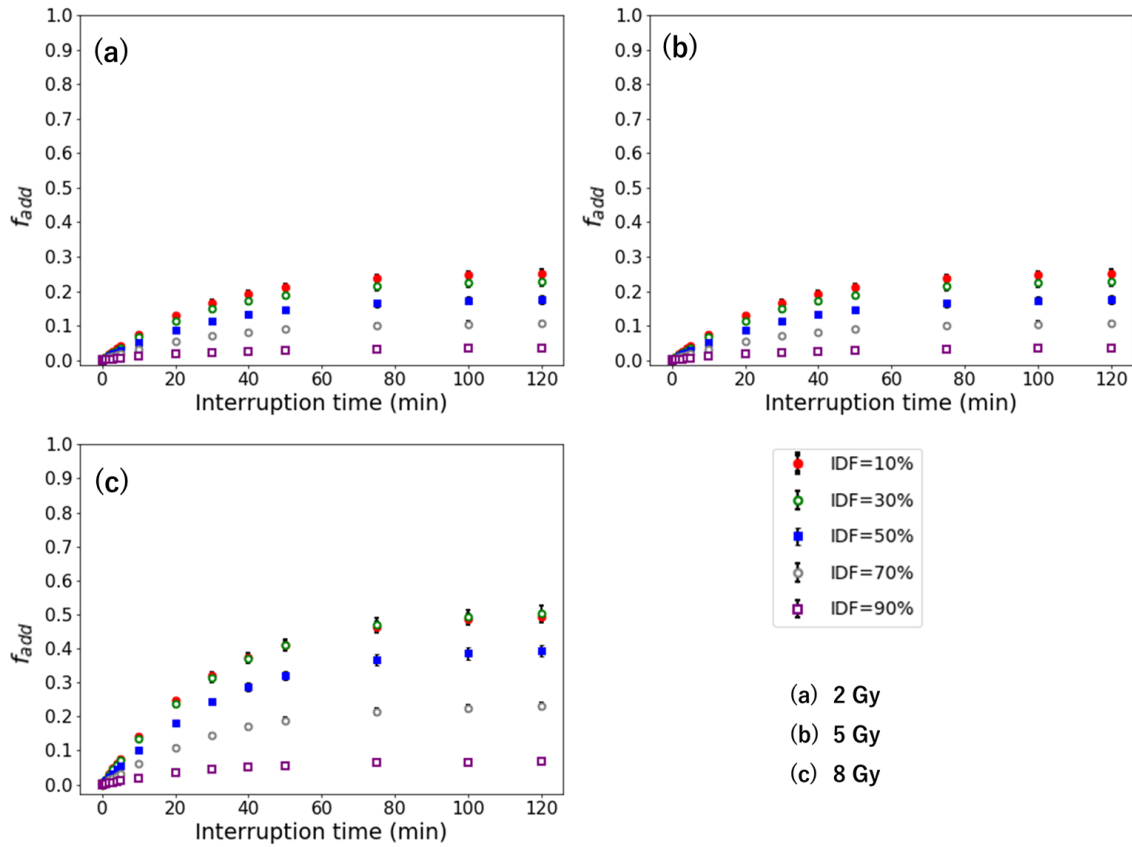


Fig. 6 f_{add} when the interruption occurs at the IDF of 10%–90% for the D of (a) 2 Gy, (b) 5 Gy, and (c) 8 Gy.

3.5. Dose compensating factor with different dose rate for interruption

Figures 7 and 8 show the f_2 and f_{add} in second-irradiation method and additional-irradiation method at the IDF of 50% with 0.5–24 Gy/min for the D of 2–8 Gy. The f_2 and f_{add} are larger with high-dose rate, which indicates a similar result with the Δ . The higher D has higher f_2 and f_{add} . Its largest values are 1.43 for the f_2 and 0.43 for the f_{add} at 8 Gy with 24 Gy/min.

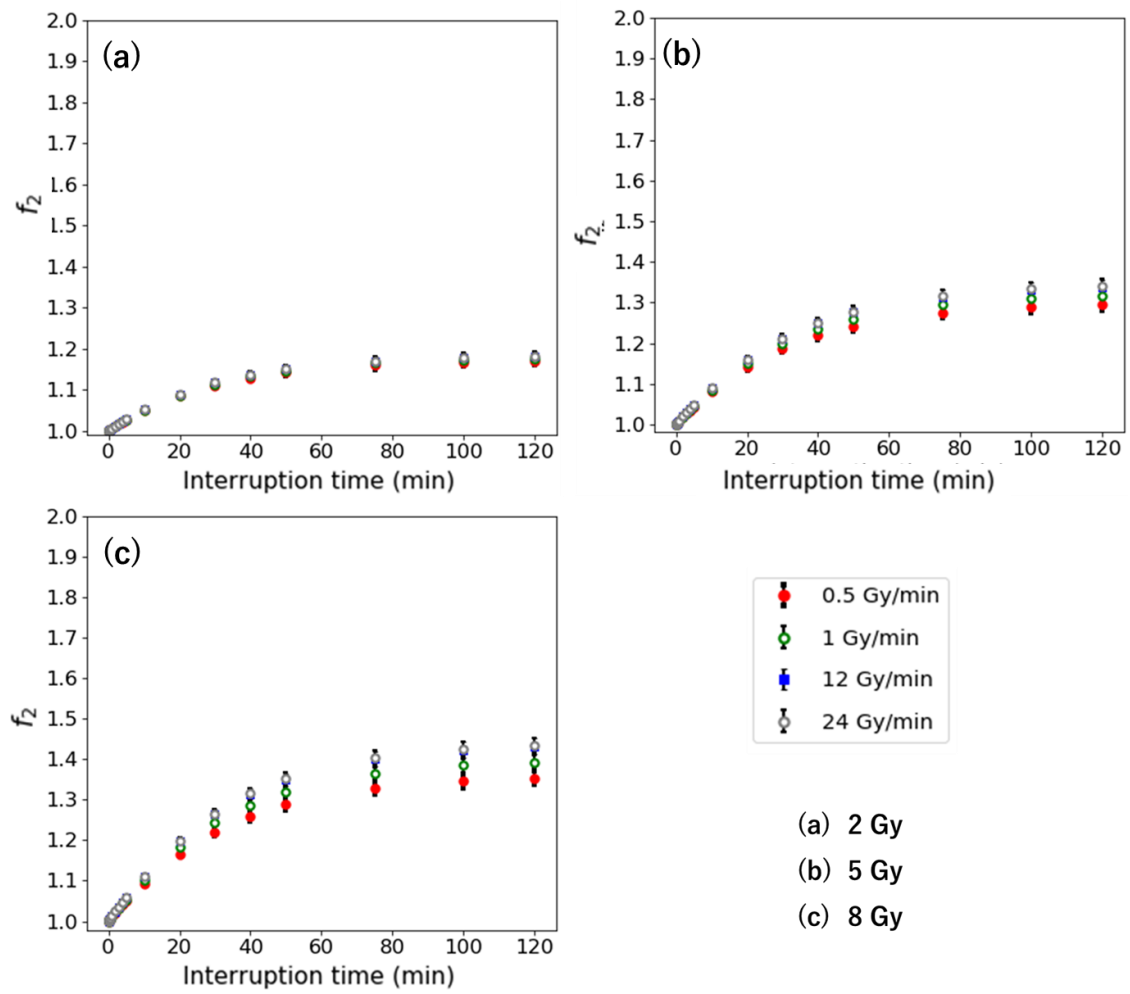


Fig. 7 f_2 vs. interruption time with 0.5–24 Gy/min for the D of (a) 2 Gy, (b) 5 Gy, and (c) 8 Gy.

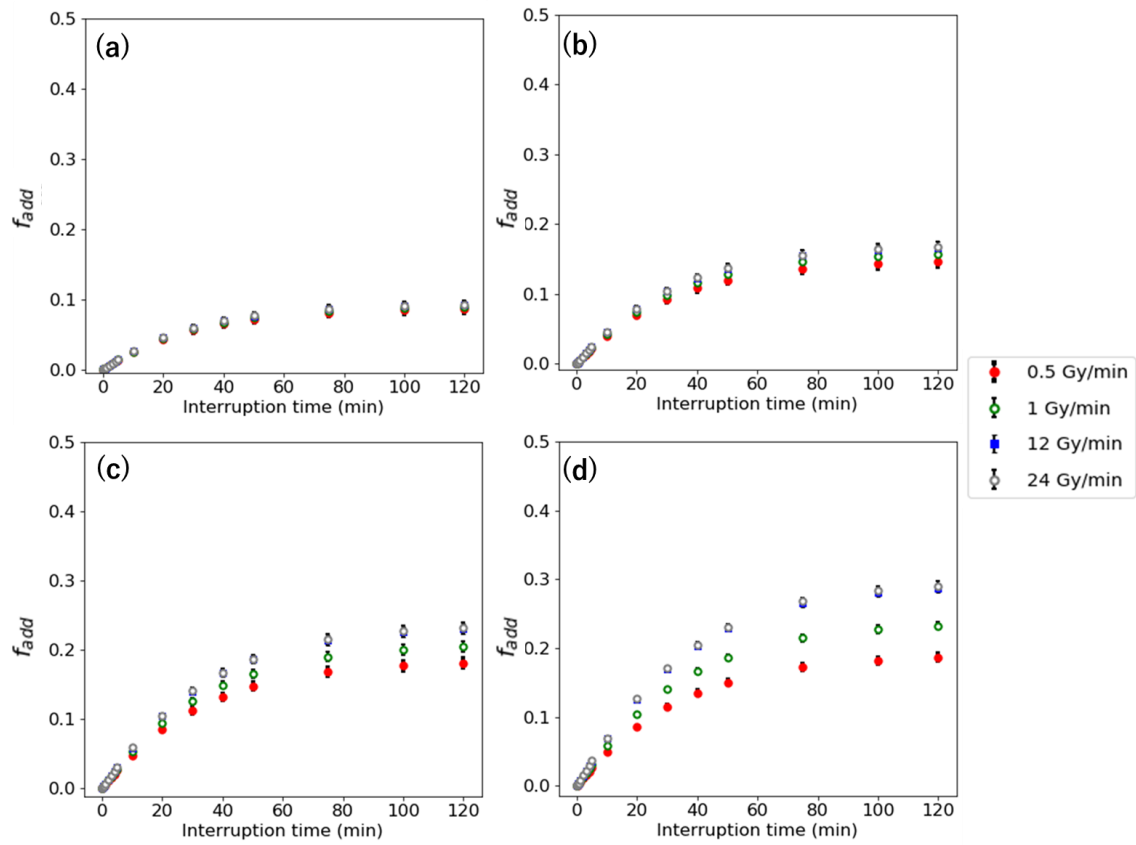


Fig. 8 f_{add} vs. interruption time with 0.5–24 Gy/min for the D of (a) 2 Gy, (b) 5 Gy, and (c) 8 Gy.

4. Discussion

The present study reveals that the biological effect of SLDR due to interruption time during photon radiotherapy was significant. The unexpected decrease of the biological effectiveness, which was compensated with the physical dose that was defined as the dose that should be added after the interruption. A previous study revealed that the SLDR occurred between interruption times of 2–3 min, or longer [32]. The current study showed that the biological dose difference with and without interruption was over 3% at the interruption, that is longer than 3 min for all of the *D*. Benedict et al. estimated the biological effectiveness with an interruption for stereotactic radiosurgery in vitro [33]. They reported that the effect of radiation decreased by 9–14% at 8 Gy when the treatment time elongates by 30 min. In the current study, a similar decrease in the biological effectiveness occurred. Additionally, the current study showed that the biological dose difference depends on the dose per fraction, dose rate, and the dose before and after interruption.

The interruption time of the biological dose difference with and without interruption at over 3% was 10 min with 8 Gy with 1 Gy/min. For radiation therapy techniques, a previous study reported the dose delivery time for bladder cancer with 2 Gy of dose per fraction, which was 2.25 min with three-dimensional radiotherapy (3DCRT),

4.29 min with IMRT, and 1.14 min with volumetric-modulated arc therapy (VMAT) [34].

405 Thus, the difference of the biological dose with and without interruption was within 3% with 2 Gy for all of the radiotherapy techniques. Ong et al. reported that the dose delivery time was 11.6 min for 3DCRT, 12 min for IMRT, and 3.9 min for VMAT for hypofraction radiotherapy [35]. Although the delivery time includes the beam-on time and interruption time, the difference of the biological dose with and without interruption for VMAT is within 3% even if the delivery time is almost composed of the interruption time. On the other hand, the biological dose difference with and without interruption is possible to be over 3% for 3DCRT and IMRT in hypofraction radiotherapy. Moreover, the interruption could occur once if there are issues with the machine, hardware, and patient in clinical practice. For the decrease of the biological effectiveness with the interruption by 415 complexity irradiation method or machine failures, the current study proposed the dose compensation model of the second-irradiation method and additional-irradiation method. Recently, the treatment technique has been advanced and multiple-direction beam with non-uniform beamlets at each segment or doses at each voxel is used in clinical [36]. Second-irradiation method was assumed that the dose profile at first irradiation is the same with second irradiation. Thus, it may be difficult to apply the second irradiation 420 method. On the other hand, to apply the additional-irradiation method in clinical, the

prompt irradiation that minimized the treatment interruptions after second irradiation.

Recently, flattening filter-free beams have been able to provide improved clinical throughput since they exhibit a high dose rate compared with the flattening filter (FF) beams. Turner et al. demonstrated that the greater impact of higher dose rates has been confirmed in a study report concerning irradiated mice [37]. Although increasing interruption time caused an increase in the delivery time, the effect of the dose rate for the difference of the biological dose with and without interruption was larger with a high dose per fraction. Therefore, the dose compensating model requires adjustment according to the dose rate.

There were limitations in our dose compensating model. Mu et al. reported that the prolonged fraction delivery time within the time frame for complex radiotherapy techniques, such as IMRT and hypofraction radiotherapy, can decrease the biological effectiveness [38]. The biological effect by the accumulation of the small dose with the interruption could be insignificant. Our study could not evaluate the Δ for certain interruptions; this demands further evaluation and research. Additionally, our simulation was performed with only an HSG tumor cell; thus, it is necessary for the Δ should be evaluated with other tumor or normal cells. The current study incorporated the SLDR. The range of the interruption time is within the t_r in which the biological effect of SLDR

occurs. The other repair such as potentially lethal damage repair is not considered in the current study. Moreover, Carlson et al. investigated the correlation of the cell kill and regions of hypoxia for conventional fractionation and hypofraction radiotherapy [37]. The other factors of the biological effects, such as tumor hypoxia and tumor repopulation, are beyond the scope of this study. Although the current study evaluated the biological effectiveness due to the SLDR by the interruption in a simulation study, portions of it are in agreement with previous experimental studies. For clinical purposes, the biological effectiveness due to interruption is difficult because existing treatment planning systems could not perform the biological dose calculation using MKM. Our proposed model with physical dose can be compensated for the biological dose difference without biological dose calculating if the decrease of the biological effect occurs due to interruption. Although the current study focused on the point prescription method, IMRT uses volume prescription that the dose was accumulated at each of voxels [39]. To apply the biological dose compensation model in volume prescription, a further study which assesses the compensating factor at each of voxel in the voxel is needed.

5. Conclusions

The interruption caused the loss of biological effect. The dose compensation model
460 could correct an unexpected decrease of the biological effectiveness with interruption
time.

465

470

475

References

1. Hoogeman MS, Nuyttens JJ, Levendag PC, et al. Time dependence of intrafraction patient motion assessed by repeat stereoscopic imaging. *Int J Radiat Oncol Biol Phys*. 2008 Feb 1; 70(2):609-18.
- 480 2. Linthout N, Bral S, Van de Vondel I, et al. Treatment delivery time optimization of respiratory gated radiation therapy by application of audio-visual feedback. *Radiother Oncol*. 2009 Jun;91(3):330-5.
3. Vladimir D, Ivana H. Evaluation of Downtime of Linear Accelerators Installed at Radiotherapy Departments in the Czech Republic. *World Congress on Medical*
485 *Physics and Biomedical Engineering* 2018; 351-354.
4. Physical considerations in the use of intensity modulated radiotherapy to produce three-dimensional conformal dose distributions. *J Jpn Soc Ther Radiol Oncol*, 2000; 12: 191-203
5. Elkind MM, Sutton H. Radiation response of mammalian cells grown in culture. 1. Repair of X-ray damage in surviving Chinese hamster cells. *Radiat Res*. 1960
490 Oct;13:556-93.
6. Mu X, Löfroth PO, Karlsson M. The effect of fraction time in intensity modulated radiotherapy: theoretical and experimental evaluation of an optimisation problem.

Radiother Oncol. 2003 Aug;68(2):181-7.

- 495 7. Curtis SB. Lethal and potentially lethal lesions induced by radiation—a unified repair
model. Radiat Res. 1986;106:252–70.
8. Tobias C. The repair–misrepair model in radiobiology: comparison to other models.
Radiat Res. 1985;8 S77–95.
9. Hawkins RB. A statistical theory of cell killing by radiation of varying linear energy
500 transfer. Radiat Res. 1994;140:366–74.
10. Hawkins RB. A Microdosimetric-Kinetic Model of cell death from exposure to
ionizing radiation of any LET, with experimental and clinical applications. Int J
Radiat Biol. 1996 Jun;69(6):739-55.
11. Rossi HH, Zaider M, Turner JE. Microdosimetry and its Applications. Berlin:
505 Springer; 1996.
12. Matsuya Y, Ohtsubo Y, Tsutsumi K, et al. Quantitative estimation of DNA damage by
photon irradiation based on the microdosimetric-kinetic model. J Radiat Res. 2014
May;55(3):484-93.
13. Inaniwa T, Kanematsu N, Suzuki M, Effects of beam interruption time on tumor
510 control probability in single-fractionated carbon-ion radiotherapy for non-small cell
lung cancer. Phys Med Biol. 2015 May 21;60(10):4105-21.

14. Nakano H, Kawahara D, Ono K, et al. Effect of dose-delivery time for flattened and flattening filter-free photon beams based on microdosimetric kinetic model. *PLoS One* 2018;13:e0206673.
- 515 15. Brenner DJ, Hlatky LR, Hahnfeldt PJ et al. The linear–quadratic model and most other common radiobiological models result in similar predictions of time–dose relationships. *Radiat Res* 1998;150:83–91.
16. Inaniwa T, Suzuki M, et al. Effects of dose-delivery time structure on biological effectiveness for therapeutic carbon-ion beams evaluated with microdosimetric kinetic model. *Radiat Res.* 2013;Jul;180(1):44-59.
- 520 17. Kase Y, Kanai T, Matsumoto Y, et al. Microdosimetric measurements and estimation of human cell survival for heavy-ion beams. *Radiat Res.* 2006 Oct;166(4):629-38.
18. Okamoto H, Kanai AT, Kase Y, et al. Relation between Lineal Energy Distribution and Relative Biological Effectiveness for Photon Beams according to the Microdosimetric Kinetic Model. *J. Radiat. Res.*, 52, 75–81 (2011).
- 525 19. Constantin M, Perl J, LoSasso T, et al. Modelling the TrueBeam linac using a CAD to Geant4 geometry implementation: dose and IAEA - compliant phase space calculations. *Med Phys.* 2011;38(7):4018–24.
20. Rogers DW, Walters B, Kawrakow I. BEAMnrc users manual. National Research

- 530 Council of Canada Report PIRS-0509(A) revL. Ottawa, Canada: NRCC; 2016.
21. Kawahara D, Nakano H, Ozawa S, Relative biological effectiveness study of Lipiodol based on microdosimetric-kinetic model. *Phys Med*. 2018 Feb;46:89-95.
22. Sato T, Watanabe R, Niita K. Development of a calculation method for estimating specific energy distribution in complex radiation fields. *Radiat Prot Dosimetry*. 2006;122(1-4):41-5. Epub 2006 Nov 28. Epub 2006 Nov 28.
- 535 2006;122(1-4):41-5. Epub 2006 Nov 28. Epub 2006 Nov 28.
23. Ma L, Men Y, Feng L. A Current Review of Dose-escalated Radiotherapy in Locally Advanced Non-small Cell Lung Cancer. *Radiol Oncol*. 2019 Mar; 53(1): 6–14.
24. Shien G, Jie Y, et al. Stereotactic body radiation therapy for centrally-located lung tumors. *Oncol Lett* 2014;7:1292–1296.
- 540 25. Uematsu M, Shioda A, et al. Computed tomography-guided frameless stereotactic radiotherapy for stage I non-small cell lung cancer: a 5-year experience. *Int J Radiat Oncol Biol Phys* 2001;51:666–70.
26. Kocher M, Treuer H, Voges J, et al. Computer simulation of cytotoxic and vascular effects of radiosurgery in solid and necrotic brain metastases. *Radiother Oncol*. 2000;54:149–156.
- 545 2000;54:149–156.
27. Ravichandran R, Binukumar JP, Davis CA1, et al. Total body irradiation (TBI): Preliminary experience on clinical implementation.. *J Med Phys*. 2013 Oct;38(4):210-

1.

28. Dubois L, Biemans R, Reniers B1, et al. High dose rate and flattening filter free
550 irradiation can be safely implemented in clinical practice. *Int J Radiat Biol.*
2015;91(10):778-85.
29. Kuterdem H, Cho P S, Marks P et al. Comparison of Leaf Sequencing Techniques:
Dynamic vs. Multiple Static Segments. *Wide Area Networking for Radiotherapy
Services* (pp.213-215).
- 555 30. McCarroll R, Youssef B, Beadle B, et al. Model for Estimating Power and Downtime
Effects on Teletherapy Units in Low-Resource Settings. *J Glob Oncol.* 2017 Jan
11;3(5):563-571.
31. Ando K, et al (2001) Relative Biological Effectiveness of the 235 MeV Proton Beams
at the National Cancer Center Hospital East. *J Radiat Res* 42: 79–89.
- 560 32. Shibamoto Y, Ito M, Sugie C, Recovery from sublethal damage during intermittent
exposures in cultured tumor cells: implications for dose modification in radiosurgery
and IMRT. *Int J Radiat Oncol Biol Phys.* 2004 Aug 1;59(5):1484-90.
33. Benedict SH, Lin PS, Zwicker RD, et al. The biological effectiveness of intermittent
irradiation as a function of overall treatment time: development of correction factors
565 for linac-based stereotactic radiotherapy. *Int J Radiat Oncol Biol Phys.* 1997 Mar

1;37(4):765-9.

34. Foroudi F, Wilson L, Bressel M, A dosimetric comparison of 3D conformal vs intensity modulated vs volumetric arc radiation therapy for muscle invasive bladder cancer. *Radiat Oncol*. 2012 Jul 23;7:111.
- 570 35. Ong CL, Verbakel WF, Cuijpers JP, et al. Stereotactic radiotherapy for peripheral lung tumors: a comparison of volumetric modulated arc therapy with 3 other delivery techniques. *Radiother Oncol*. 2010 Dec;97(3):437-42.
36. Kim T, Zhu L, Suh TS, et al. Inverse planning for IMRT with nonuniform beam profiles using total-variation regularization (TVR). *Med Phys*. 2011 Jan;38(1):57-66.
- 575 37. Carlson DJ, Keall PJ, Loo BW, et al. Hypofractionation results in reduced tumor cell kill compared to conventional fractionation for tumors with regions of hypoxia. *Int J Radiat Oncol Biol Phys*. 2011;79:1188–1195.
38. Turner HC, Shuryak I, Taveras M, et al. Effect of dose rate on residual γ -H2AX levels and frequency of micronuclei in X-irradiated mouse lymphocytes. *Radiat Res*. 2015;183:315–24.
- 580 39. Kukolowicz PF, Mijneer BJ. Comparison between dose values specified at the ICRU reference point and the mean dose to the planning target volume. *Radiother Oncol*. 1997;42(3):271–7.

585

Fig. 1 Two types of dose compensating methods: One is second-irradiation method that the decrease of the biological effectiveness with interruption is corrected with the D_2 in the second irradiation. The other is the additional-irradiation method that the decrease of the biological effectiveness with interruption is compensated with the additional dose.

590

Fig. 2 Survival fraction vs. interruption time at the IDF of (a) 10% and (b) 50% for the D of 2–8 Gy.

595

Fig. 3 Δ when the interruption occurs at the IDF of 10%–90% for the D of (a) 2 Gy, (b) 5 Gy, and (c) 8 Gy.

Fig. 4 Δ vs. interruption time with 0.5–24 Gy/min for the D of (a) 2 Gy, (b) 5 Gy, and (c) 8 Gy.

600

Fig. 5 f_2 when the interruption occurs at the IDF of 10%–90% for the D of (a) 2 Gy, (b) 5 Gy, and (c) 8 Gy.

Fig. 6 f_{add} when the interruption occurs at the IDF of 10%–90% for the D of (a) 2 Gy, (b) 5 Gy, and (c) 8 Gy.

605

Fig. 7 f_2 vs. interruption time with 0.5–24 Gy/min for the D of (a) 2 Gy, (b) 5 Gy, and (c) 8 Gy.

Fig. 8 f_{add} vs. interruption time with 0.5–24 Gy/min for the D of (a) 2 Gy, (b) 5 Gy, and (c) 8 Gy.

610